International Journal of Fatigue 158 (2022) 106764

Contents lists available at ScienceDirect

International Journal of Fatigue

journal homepage: www.elsevier.com/locate/ijfatigue

Machine learning based very-high-cycle fatigue life prediction of Ti-6Al-4V alloy fabricated by selective laser melting

Jun Li [a], Zhengmao Yang [a,*], Guian Qian [a,b,*], Filippo Berto [c]

[a] Institute of Mechanics, Chinese Academy of Sciences, Beijing 100190, China
[b] State Key Laboratory of Nonlinear Mechanics (LNM), Institute of Mechanics, Chinese Academy of Sciences, Beijing 100190, China
[c] Department of Mechanical and Industrial Engineering, Norwegian University of Science and Technology (NTNU), Richard Birkelands vei 2b, 7491 Trondheim, Norway

ARTICLE INFO

Keywords:
Very-high-cycle fatigue (VHCF)
Machine learning
Selective laser melting (SLM)
Fatigue life prediction
Monte Carlo simulation (MCs)

ABSTRACT

Few machine learning (ML) models were applied for very-high-cycle fatigue (VHCF) analysis and these methods encounter limitations in data sparsity and overfitting. The present work aims to overcome data sparsity and propose an easy-to-use and nonredundant ML model for VHCF analysis. Monte Carlo simulation (MCs) is run to enlarge dataset size and a ML method is proposed to investigate the synergic influence of defect size, depth, location and build orientation on Ti-6Al-4V. The coefficient factor that indicates the percentage variation between the predicted and experimental fatigue lives can reach up to 0.98, meaning that the model demonstrates good prediction accuracy.

1. Introduction

Utilizing traditional methods to investigate factors that affect very-high-cycle fatigue (VHCF) of additive manufactured alloys faces a series of challenges. Unlike traditional manufacturing process which can mass produce objects, 3D printing process, though it helps create objects in a variety of shapes, is limited by the machine capabilities of 3D printers themselves. To be specific, the lead time of printing desired objects is usually long and the post-processing such as surface finishing must be considered if the precision of 3D printers cannot meet the expectation, followed by polishing process to obtain desired test samples. In terms of materials, as demonstrated in ref. [1], the expense of powdered metal is higher than bar stock. As a result, the longer duration of VHCF test compared with low/high cycle fatigue test as well as higher cost result in sparse available test data. The construction of traditional models like ref. [2–3] relies heavily on conducting a number of time-consuming and cost-intensive experiments and yet their generalization capacity is limited by the dataset size. The challenge has urged researchers to pursue new predictive methods that do not require laborious experimental work and thus machine learning (ML) approach is proposed, as an effective technique which has demonstrated its great capability of recognizing patterns in complex data for linear and nonlinear regression [4].

Titanium alloys, especially Ti-6Al-4V, are widely used in aerospace, commercial and biomedical applications because their excellent combination of high specific strength, corrosion resistance, low density, high fracture toughness, and superior biocompatibility [5–7]. Machining of titanium alloys have drawn significant attention on manufacturing and research area. Titanium alloys are often considered as hard-to-machine materials and real progress in industrial productivity is not yet visible. Growing maturity of additive manufacturing has enabled the use of rapid manufacturing technology [8–10]. Selective laser melting (SLM), as one of the laser power bed fusion methods, can reduce material waste and produce components with high complexity [11–12]. However, SLM is associated with a range of parameters such as energy density, hatch speed, scanning speed, laser power hatch distance and layer thickness and variations in these parameters may result in microstructure and defect distribution [11,13]. It is noted that effect of build orientation on mechanical properties and microstructure of Ti-6Al-4V manufactured by SLM is significant [14] and the effect of build orientation on the VHCF response of Ti-6Al-4V alloy was investigated in ref. [2]. But the synergic effect of build orientation and defect properties on fatigue life is not apparent. Derivation of relationship between the fatigue life and related fatigue properties relies on sophisticated statistical extrapolation and is often costly and time-consuming. In this work, the influence of defect properties and build orientation on the VHCF response of SLMed Ti-6Al-4V was studied. VHCF morphology and fractography data were collected by scanning electron microscopy after fully reversed ultrasonic fatigue

* Corresponding authors.
E-mail addresses: zmyang@imech.ac.cn (Z. Yang), qianguian@imech.ac.cn (G. Qian).

https://doi.org/10.1016/j.ijfatigue.2022.106764
Received 25 April 2021; Received in revised form 27 November 2021; Accepted 21 January 2022
Available online 24 January 2022

tests.

ML models for fatigue prediction have been increasingly proposed to solve complex linear and non-linear relationships. Random forest (RF), support vector regression (SVR) and the artificial neural network (ANN) are three commonly used regression algorithms to carry out fatigue life prediction. Each of these three algorithms has its own drawback. The prediction accuracy of random forest decreases with number of decision trees and more trees may result in longer processing time [15]. For support vector regression algorithm, it can generate results of high accuracy and generalizability when the training data is not massive [16]. Since in the work a large data set will be generated and short training time is desired, the ANN algorithm has been chosen. The ANN which is one of the most extensively employed ML algorithms has long been used to predict the S-N relation [17] and it shows distinguished performance in the mapping complicated nonlinear relationships [18,19]. Back-propagation ANN is applied to model the nonlinear relationship among variables.

As noted, the number of publications of VHCF of SLMed Ti-6Al-4V is not abundantly available and the lack of fatigue data is an inevitable issue to confront with [2,20]. Overfitting is a common issue that prevents the ML algorithms from generalizing models to fit the observed data as well as unseen data. Variations of fatigue properties also add to the difficulty of set up an ANN model.

Probabilistic models of fatigue life distribution under various related factors are usually proposed to address the increasing concern for structural reliability and integrity assessment of engineering fields. A probabilistic stress-life (P-S-N) curve is developed by a finite number of fatigue tests to analyze the effect of scatter and estimate an average S-N curve with standard deviation. Finite element simulation and statistical methods such as Weibull distribution are widely applied in probabilistic fatigue life analysis [21–25]. For Weibull distribution, P-N relationship should be first experimentally determined and then based on shape parameter and scale parameters, a P-S-N diagram can be established to estimate confidence bands. The assumption of P-S-N is that a sufficient number of identical test specimen are run until failure and then the probability of failure can be obtained by analyzing the scatter of fatigue lives. At each stress level, SLMed specimen for each build orientation only has limited data available and thus it is difficult to determine Weibull distribution parameters. The constructed Weibull distribution may be shifted to the left or right side of the actual distribution in this case.

To compensate the effects of overfitting and shifted variations, a Beta-PERT type Monte Carlo simulation (MCs) is applied to enlarge dataset size. The MCs is useful for randomly generating numbers of a variable within a given range according to a probability density function [26,27]. Furthermore, the Beta-PERT distribution can generate probabilistic model based on optimistic values and confidence bands and adjust the skewness of the distribution curve to compensate the shift of distribution curves. After MCs, the ANN model is constructed, trained, and validated with the data generated to predict fatigue life based on defect properties and build orientation.

In the present work, the motivation is to overcome data sparsity and present a convenient and nonredundant ML method for the VHCF life prediction of SLMed Ti-6Al-4V. The ease of implementation and simplicity of ML models were often forsaken when constructing ML models. Recently, there is a trend to build an ANN model with multiple layers and scores of neurons which is also called deep neural network (DNN). But the increasing layers and neurons only add to limited improvement of accuracy [28] while the processing time of the ML model may double or triple. The redundant DNN is user-unfriendly and can be truncated to a shallower ANN. In this context, a shallow ANN is proposed. The defect properties including (equivalent) defect size, location (distance to surface), and depth (fracture surface roughness measured by scanning white light interferometry) together with build orientation will be correlated with the VHCF life through ANN. The predictive fatigue life will be analyzed, and performance of the model will be evaluated.

2. Construct raw dataset

2.1. Specimen and test procedure

2.1.1. Material

The material used in this work is a type of titanium alloy which is Ti-6Al-4V. As additive manufacturing techniques has enabled titanium alloy to become a cost-effective material, there is an increasing attention to the structural integrity of additively manufactured Ti-6Al-4V components. It is important to better understand the failure mechanisms subjected to cyclic loadings. The test samples are made by SLM and different build orientations are achieved by cutting the bulk 3D printed material in corresponding angles which are 0°, 45°, and 90°, as shown in Fig. 1. (a)[2]. The process technique employed for manufatcuring the samples makes the defects well distributed inside the specimens rather than on the specimen surface.

2.1.2. Specimen and fatigue test

Fig. 1(b) shows the test specimen geometry. An ultrasonic fatigue tester (Lasur GF20-KT) was used to carry out the fatigue tests at $R = -1$ with a frequency of 20 kHz ± 500 Hz at room temperature in air. Three groups of specimen with respect to build orientations were used for ultrasonic fatigue test. The range of stress amplitude varies from 500 MPa to 200 MPa which contains high cycle fatigue and VHCF regimes (will be shown in Fig. 8) and fatigue limits do not appear for all of three configurations. Above 250 MPa, each of three groups of specimen with different build orientations were tested every 50 MPa and below 250 MPa, they were tested every 25 MPa. All the fatigue data were evaluated

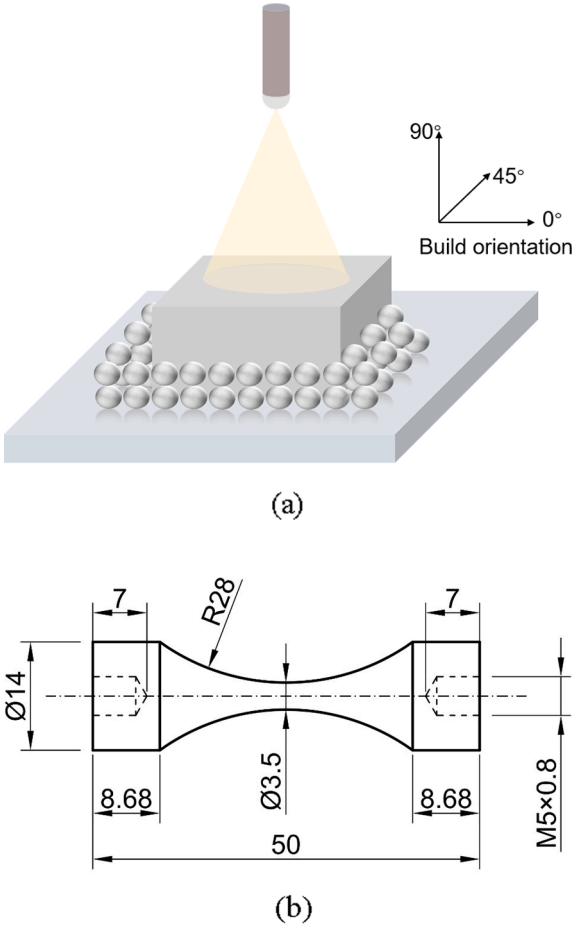

Fig. 1. (a) Schematic drawing of SLMed Ti-6Al-4V (b) test specimen geomerty.

after the fatigue failure. More details on the fatigue test could be referred in [2].

2.2. Raw data collection

Fig. 2 shows the flowchart of ML process in predicting fatigue life with the synergic effect of build orientation and defects. Before applying any predictive model to the fatigue test data collected, the data preparation process must be considered since most ML algorithms learn from the data provided and thus it is imperative that to construct a well-structured dataset. The raw data were obtained from the article [2]. The raw dataset, which is listed in Table 1, consists of S-N and defect properties of 22 samples representing seven horizontally built, eight 45° built and seven vertically built titanium alloy samples, respectively. All specimens were manufactured through SLM and different build orientations of specimens were achieved by cutting bulk 3D printed material in corresponding angles. Defect depth, size and distance to surface were observed using scanning white light interferometry and scanning electron microscopy.

2.3. Feature selection

The realization of a ML model depends on the selection of features. Relevant features are selected to improve model accuracy and reduce overfitting and training time. As shown in Fig. 3, SLMed specimens in different directions show similar microstructure but their strength and defect properties such as defect size and distribution, are quite different and these SLMed defect properties have effects on their VHCF life [2,3,29,30]. The dataset consists of five inputs and one output. The inputs include material defect properties (defect depth, defect size and defect distance from surface), fatigue loading (maximum stress), and build orientation and the output is the predicted fatigue life.

3. Data preparation

3.1. Monte Carlo simulation and discussion

The S-N data collected are imported to *Matlab Regression* tool to generate fit curve equations to obtain the Basquin relation, $\Delta\sigma N_f^{-a} = C$, while fatigue loadings and defect properties relation are generated using *Microsoft Excel* regression tool after outliers were removed. While the raw dataset was constructed, the sizes of subsets for every fatigue feature are too few to achieve a desirable level of performance since sparse data is given by the article [2]. Sparse data add to the difficulty of generalization of a ML predictive model since a model with a small dataset often encounter overfitting which means that a model learns from the dataset too well so that the accuracy of new predictions beyond the dataset is undermined. The scatter or variability of features makes the overfitting more likely to occur for models with small dataset and makes the generalization of the predictive model very poor.

Scatter is one of the most common phenomena of mechanical and fatigue properties of materials. The S-N relationship of fatigue data exhibits the scatter phenomenon. To illustrate, for a certain fixed amplitude loading or stress level, the variability in titanium alloy's inherent material properties, defect properties such as defect size, and poor alignment of test machine and samples can cause the fatigue lives of seemingly identical specimens to vary [31]. To compensate for the negative effects of limited available data, data generation techniques can be applied to the original dataset to increase the amount of data in dataset. The scatter of fatigue and mechanical features exhibit Gaussian-like distribution. With that determined, the MCs method can be applied to the original dataset to yield a range of possible outcomes with the

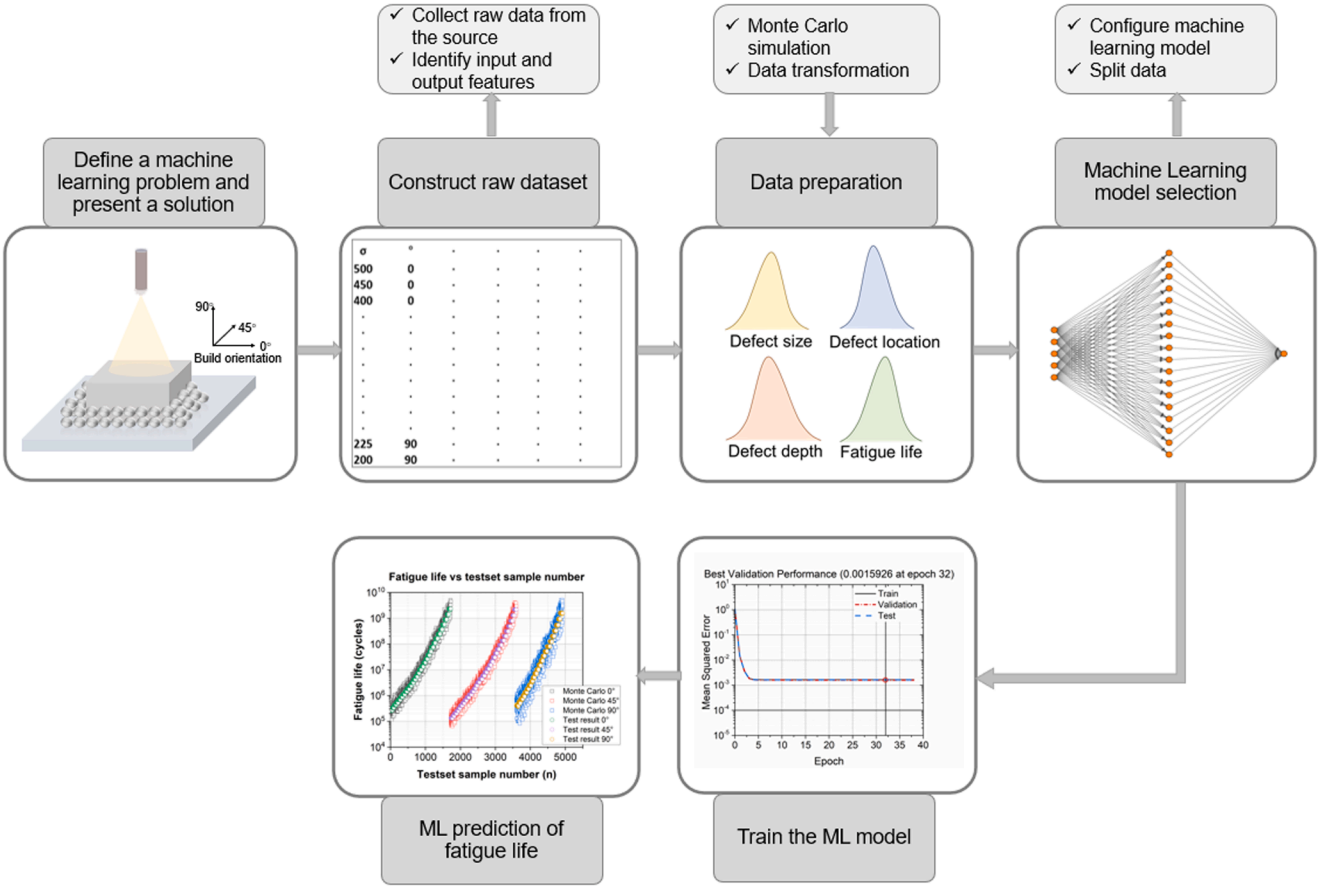

Fig. 2. Machine learning process flowchart of predicting fatigue life with the synergic effect of build orientation and defects.

Table 1
Build Orientation, defect properties, σ_{max} (maximum stress), and fatigue life, collected from [2].

Sample ID	σ_{max} (MPa)	Build orientation (°)	Defect depth (μm)	Defect size (μm)	Distance to surface (μm)	N_f (cycle)
1	500	0	74	115	200	1.10E + 05
2	450	0	23	51	922	2.68E + 06
3	400	0	33	56	1043	5.35E + 06
4	350	0	56	69	589	1.10E + 07
5	300	0	49	95	751	2.51E + 07
6	250	0	30	42	273	2.40E + 08
7	225	0	128	30	627	5.10E + 08
8	450	45	36	50	250	3.70E + 05
9	400	45	50	93	1051	7.45E + 05
10	350	45	27	39	344	9.23E + 06
11	320	45	61	35	332	3.10E + 07
12	300	45	57	28	449	7.18E + 07
13	250	45	65	80	204	8.68E + 07
14	225	45	36	64	297	3.41E + 08
15	200	45	70	48	145	5.35E + 08
16	400	90	29	110	827	2.15E + 05
17	350	90	53	62	343	3.97E + 06
18	320	90	23	83	85	9.78E + 06
19	300	90	27	39	299	2.38E + 07
20	250	90	83	72	1303	1.03E + 08
21	225	90	44	64	399	1.42E + 08
22	200	90	85	29	302	2.11E + 08

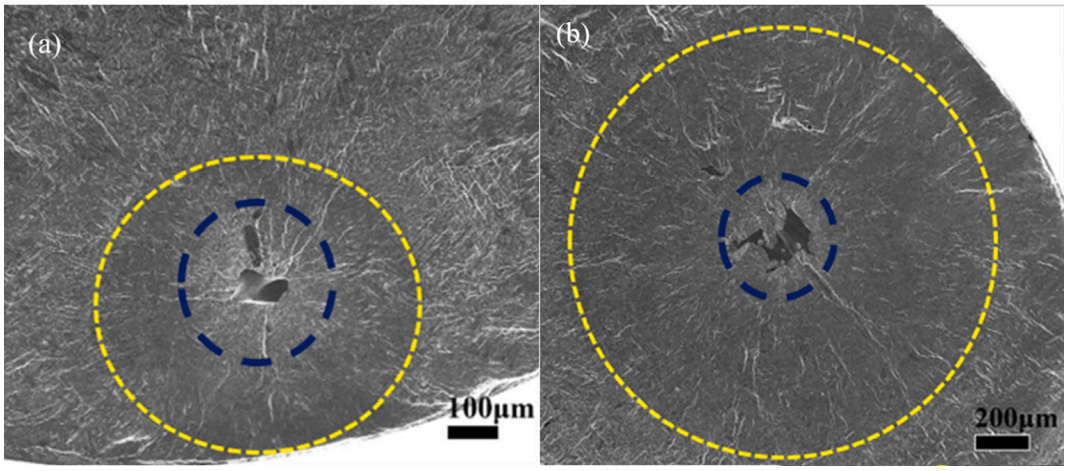

Fig. 3. Fractography of Ti-6Al-4V specimens manufactured by SLM with different build orientations [2] (a) 45°, $\sigma_a = 450$ MPa and $N_f = 3.7 \times 10^5$; (b) 90°, $\sigma_a = 400$ MPa and $N_f = 2.15 \times 10^5$.

same probabilities of each feature.

The first step in MCs is to identify the statistical distribution model for each set of input parameters. Then based on the requirements of the statistical distribution model chosen, random samples will be extracted from the outputs of the MCs model. One of the most widely used MCs is the normal distribution model. However, to build a typical normal distribution model, the standard deviation and the mean value must be provided to describe the variation from the mean. Apparently, there is great difficulty in identifying the mean and standard deviation of the MCs model since sparse data could result in huge percentage of error. Therefore, other models that do not require standard deviation to produce outputs are desired. The simplest model that suits the condition is the triangular distribution. The triangular distribution is a continuous probability distribution which shapes like a triangle with minimum, maximum, and most likely values as its bounds [32]. Unlike the normal distribution, the triangular distribution emphasizes the most likely value or the mode value. The shape of triangle may be skewed to the left or right depending on the mode value. The disadvantage of this model is that it may overemphasize the mode value at the expense of minimum or maximum values and thus the accuracy of the results may be jeopardized. The beta-PERT distribution [33] is another model that is also defined by minimum (a), maximum (c) and the most likely values (b) but compared with the triangular distribution it yields a distribution that more similarly represents the realistic probability distribution. The appeal of the beta-PERT distribution is that, depending on the reliability of the input parameters, the beta-PERT distribution can closely resemble the normal or lognormal distributions. To determine the most likely value, the raw dataset is imported to the *matlab* and *Excel* using the built-in regression tool to obtain linear and non-linear relationships. The points on the regression lines are considered the most likely values. Parallel lines are also made passing through the lowest and highest points in the raw dataset to determine the lower bound and upper bound of the model. As the bounds and mean values are collected, the shape parameters α, β and standard deviation σ would be calculated using the equations below:

$$\alpha = \frac{4(b-a)}{c-a} + 1 \tag{1}$$

$$\beta = \frac{4(c-b)}{c-a} + 1 \tag{2}$$

$$\sigma = \frac{c-a}{6} \tag{3}$$

where a is the minimum value or lower bound; b is the optimistic value or regression value; c is the maximum value or upper bound.

In the following step, the MCs is run in *Excel* to augment the dataset size for stress amplitude regimes from 190 MPa to 460 MPa. For Ti-6Al-4V alloy that is printed in 90°, when stress amplitude is greater than 410 MPa, there is no apparent defect depth detected and therefore the stress amplitude range is adapted to the range from 190 MPa to 410 MPa. For every 10 MPa, 400 random data points are generated for each fatigue feature and 32,800 data points are generated in total.

The standard deviation of MCs results in Table 2, to a large extent, depends on the dispersion of original defect data. Raw defect data exhibits significant variability against fatigue life and stress and thus the trend of regression line for each defect property is greatly influenced by outliers and extreme values. To deal with the uncertainty, outliers and extreme values were removed before running regression and yet this process could potentially cause errors in judging the trend of regression and yield greater dispersion for MCs results. For defect size of specimens that are manufactured in 45°, the variability is too high to determine the trend of regression even if the outliers and extreme values were removed. So, in this situation, the relation between the defect size and stress is considered as a piece-wise function. It is assumed that before the threshold 275 MPa, defect size and stress are correlated in a positive relationship, and after threshold value, these factors exhibit a positive relationship with a different trend.

3.2. Data transform

Before choosing any ML model, it is of great significance to transforming data collected. For application of VHCF prediction model, the training time is expected to be very time-consuming and to avoid this, in this work, the scale of the VHCF life is extremely high compared with that of low cycle fatigue life and thus the training time would be very long if no data preprocessing techniques are applied to the fatigue life data. Data normalization as a result is crucial to expedite the training time by scaling down the data to the same range [34]. The data generated by MCs are mapped into a range [0, 1] and the transformation equation is given by Eq. (4).

$$X_N = \frac{X - X_{min}}{X_{max} - X_{min}} \tag{4}$$

where X_N is the normalized value of the corresponding X , X_{max} and X_{min} are the maximum and minimum value of the X , respectively.

4. ML model selection

4.1. Backpropagation neural network model based on L-M algorithm

The backpropagation neural network has already been applied in the various fields such as fatigue analysis and ecology and it has demonstrated strong capability of interpolating non-linear relationship between the inputs and outputs [35–36]. The feedforward neural network model with backpropagation based on Levenberg-Marquardt algorithm is used in the present work, as shown in Fig. 4. The backpropagation model architecture that consists of 3 layers was established to predict the VHCF life of Ti-6Al-4V alloy. The defect distance to surface, build orientation, defect depth and defect size were used as inputs and VHCF life was the output. The network contains three components: one input layer with 5 nodes, one hidden layer with 18 nodes and one output layer with 1 node.

Table 2
Variation of Monte Carlo simulation.

Monte Carlo simulation results		Standard deviation
Defect depth	0°	11.4
	45°	5.6
	90°	7.49
Defect size	0°	11.6
	45°	0
	45°	0.72
	90°	7.7
Defect distance to surface	0°	68.7
	45°	30.7
	90°	41.0

Traditionally, the backpropagation model is based on the gradient descent algorithm to minimize the error by calculating the minimum gradient of the error curve [37]. The weights and biases in the forward direction are randomly initialized and the in backward direction the gradient descent algorithm is performed to minimize the error to the desired level. However, in terms of medium size training set, the training speed and convergence of the traditional gradient descent algorithm may take extremely long time. The Levenberg-Marquardt algorithm interpolates between the Gauss–Newton algorithm and the method of gradient descent and it significantly outperforms simple gradient descent and conjugate gradient descent methods for medium sized problems [38]. Levenberg-Marquardt algorithm is designed to solve non-linear least squares problems by minimizing the sum-of-error function of the following form:

$$E = 1/2 \sum k(e_k)^2 = 1/2||e||^2 \tag{5}$$

where $e = (e_1, e_2, \ldots, e_k)$ is a vector and is referred as residuals. If the residual between the pervious weight vector and the new weight vector is small, the error vector can be substituted by a Taylor series.

$$e_{(j+i)} = e_{(j)} + \partial e_k / \partial w_i (w_{(j+1)} - w(j)) \tag{6}$$

As a result, the error function can be transformed as:

$$E = 1/2||e(j) + \partial ek/\partial wi(w(j+1) - w(j))||^2 \tag{7}$$

Minimizing the error function in terms of new weight vector, yields

$$w_{(j+1)} = w_{(j)} - (Z^T Z)^{-1} Z^T e_{(j)} \tag{8}$$

where $(Z)_{ki} \equiv \partial e_k / \partial w_i$.

By neglecting the second term, the Hessian for the sum-of-square error function:

$$(H)_{ij} = \partial^2 E/\partial w_i \hat{A} \cdot \partial w_j = \sum \{(\partial e_k/\partial w_i)(\partial e_k/\partial w_i) + e_k \partial^2 e_k/\partial w_i \partial w_j\} \tag{9}$$

can be rewritten as:

$$H = Z^T Z \tag{10}$$

The computation of the Hessian is relatively easy for the backpropagation accommodates the network weights using first order derivatives. But there is still a concern about the new formula since it could possibly cause a large step size during the descent process causing the function fail to reach the minimum. To compensate the negative effect, a new parameter is introduced to modify the error function, which can be also called regularization.

$$E = 1/2\left|\left|e(j) + \frac{\partial ek}{\partial wi}(w(j+1) - w(j))\right|\right|^2 + \lambda||w(j+1) - w(j)||^2 \tag{11}$$

where λ is the parameter that controls the step size and $w_{(j+1)} = w_j - (Z^T Z + \lambda I)^{-1} Z^T e_{(j)}$.

Each input neuron (x_i) has an associated weight (w_i) and bias (b_i). In the hidden layer, each node transforms values from the previous layer using a linear weighted summation $w_i \cdot x_i + b_i$ and a non-linear activation function φ. The output y can be expressed as

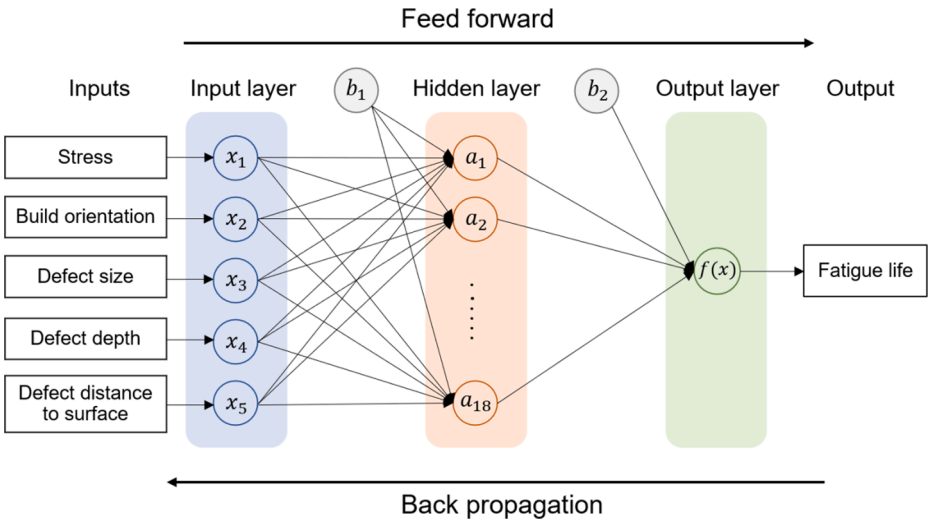

Fig. 4. The architecture of ANN with single hidden layer.

$$y = \varphi\left(\sum_{i=1}^{n} w_i \hat{A} \cdot x_i + b_i\right) \tag{12}$$

where w_i and b_i represent the weight and bias of the i^{th} neuron of input layer and n represents the number of elements in the input layer.

The activation function φ is a mathematical equation that determines the output of a neural network. Sigmoid, ReLU, and tanh functions are some frequently used functions [39–40]. The tanh or hyperbolic tangent function is chosen as the activation function in this work.

$$\varphi = \frac{e^{Z} - e^{-Z}}{e^{Z} + e^{-Z}} \tag{13}$$

Compared with the sigmoid function, the gradient of tanh function is steeper which fastens the convergence and optimization of neural network [41].

Fig. 5 represents the process of machine learning. The entire data set is randomly divided into three subsets. 70% of the 32,800 data are used for training set, 15% for validation set and 15% for test set.

5. Results and discussion

Two metrics that are used to measure the precision and evaluate the performance of the ANN model are coefficient of determination R^2 and mean-squared error (MSE).

$$R^2 = 1 - \frac{\sum_{i=1}^{n}(P_i - P_i^{pre})^2}{\sum_{i=1}^{n}(P_i - P_{mean})^2} \tag{14}$$

$$MSE = \frac{1}{n}\sum_{i=1}^{n}(P_i - P_i^{pre})^2 \tag{15}$$

where P_i is the i^{th} P in the generated dataset, P_i^{pre} is the i^{th} predicted value and P_{mean} represents the mean value of generated dataset. For the R^2, it ranges from 0 to 1. The higher R^2 is, the better fit the model is. MSE indicates the average residual between the generated dataset and predicted results. The smaller MSE, the better the predicted results. Table 3 shows that the coefficient of determination of training, validation and

Table 3
Performance of ANN model.

Data Set	MSE	R^2	R
Training Set	0.0411	0.9711	0.98545
Validation Set	0.0399	0.9716	0.98572
Test Set	0.0408	0.9711	0.98543
All	0.0409	0.9712	0.98549

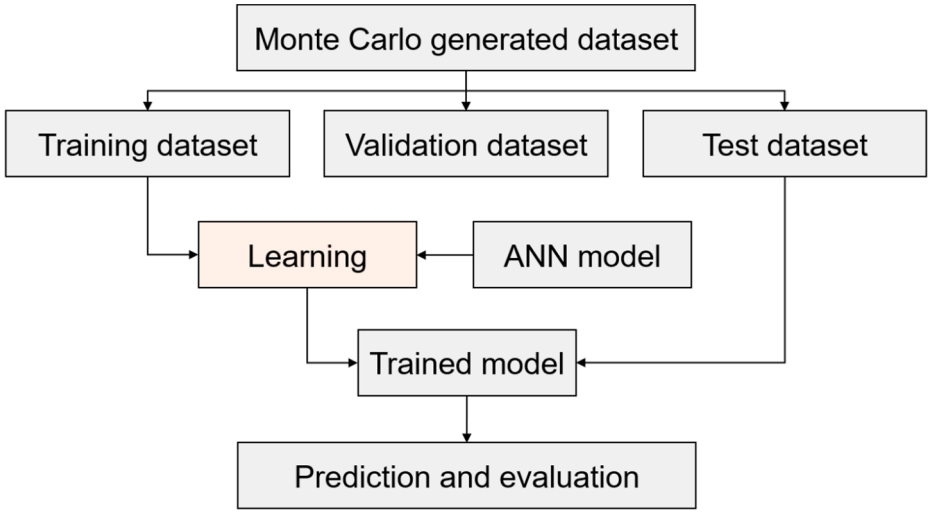

Fig. 5. Machine learning process flowchart.

test sets are 0.9711, 0.9716, and 0.9711 respectively, which are very close to 1. This means that the predicted results are in good accordance with the generated dataset, indicating that the trained ANN model has successfully interpreted the relationship between the build orientation, defect properties and VHCF property of Ti-6Al-4V alloy. The MSE for training, validation and test sets are 0.0411, 0.0399, and 0.0408, respectively. Considering the scale of the VHCF life, MSE calculated are relatively small and acceptable, implying that the predicted results are very close to the actual values. Although the MSE of test set is higher than the validation set, its accuracy remains high. Fig. 6 indicates the normalized mean-squared error versus epoch. It can be noted that the mean-squared error converges to a global optimization in a short time which means that the ML algorithm and functions chosen for the model have a good agreement with the data provided so that it reaches the minimum quickly. The R value for training, validation and test sets are above 0.98 and clearly indicates that there is high correlation between estimates and actual values.

Fig. 7 represents the result of ANN prediction. It can be seen that the predicted points form three distinguished curves representing VHCF response of SLMed Ti-6Al-4V under the effect of build orientation and defects. The predicted results have a good agreement with the true response shown in Fig. 8. The regression lines in Fig. 8 represent the Basquin relations for 0°, 45°, 90° built specimens, which are $\sigma_a = 1527N_f^{-0.09113}$,$\sigma_a = 1506N_f^{-0.09443}$, $\sigma_a = 1212N_f^{-0.08626}$ with coefficient of determinations R^2 equal to 0.9094, 0.939, and 0.9046, respectively. Some comparisons between the predicted fatigue life using ANN model and the actual fatigue life values are shown in Fig. 9 (a) and (b). In Fig. 9 (a), for better visualization of relationship between MCs testset data and predicted fatigue life data, MCs testset data at one specific stress level will be compared with the predicted fatigue life at the same stress level from 500 MPa to 200 MPa and it can be seen clearly that the test results lie within MCs testset and form regressions very close to *Matlab* regressions. In Fig. 9 (b), it is found that all samples in test set fall along diagonal which is the equal life line and fall within 95% confidence interval in ref. [2]. It seems that the data generated by MCs represent the feature of the original data well. The S-N regression line obtained by ANN model has relatively small difference with the S-N curve obtained from ref. [2]. Large dataset size prevents the occurrence of overfitting and underfitting since small dataset size causes the ML model to fit too well to the data given and fail to predict results beyond the dataset. The generalization ability of the ANN model is promising in digesting new data and making accurate predictions given defect properties and build orientation.

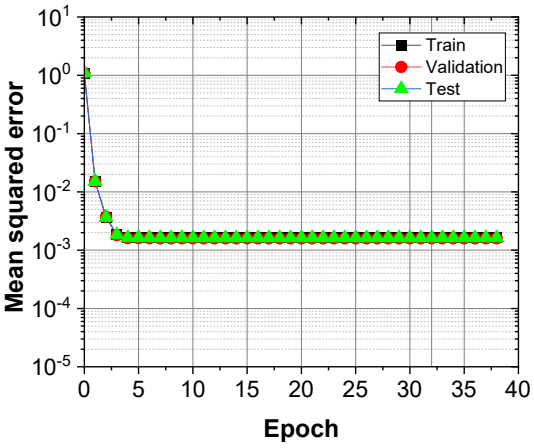

Fig. 6. Mean square error of normalized data versus epoch.

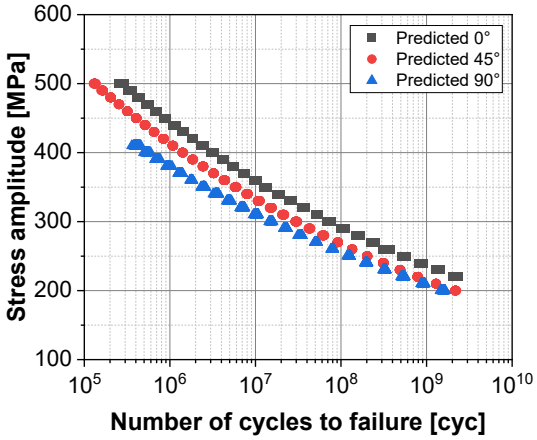

Fig. 7. Predicted fatigue life based on the ANN model.

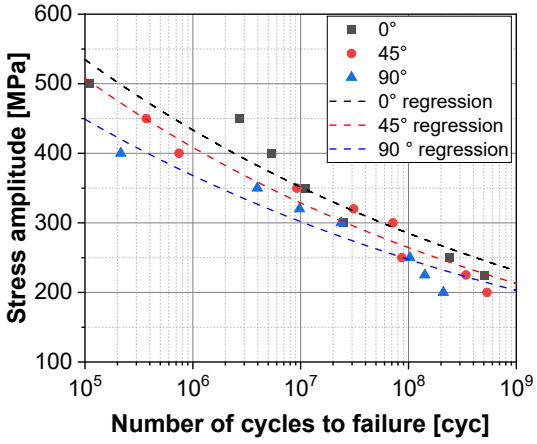

Fig. 8. S-N graph retrieved from [2]. ($0^\circ : \sigma_a = 1527N_f^{-0.09113}$,.$R^2 = 0.9094$; $45^\circ : \sigma_a = 1506N_f^{-0.09443}, R^2 = 0.939; 90^\circ : \sigma_a = 1212N_f^{-0.08626}, R^2 = 0.9046$)

6. Conclusions

This work examined the backpropagation neural network machine leaning method for modelling the very-high-cycle fatigue life of additively manufactured Ti-6Al-4V alloy. Important features are primarily identified in terms of defect size, defect distance to surface, defect depth and build orientation. The main conclusions can be drawn from the results obtained above:

(1) The Monte Carlo simulation is an effective method to enlarge dataset size while preserving the interrelationship between features. The difficulty in obtaining large amount of fatigue data of the additively manufactured Ti-6Al-4V alloy is solved by random number generation technique. More representative data are obtained, and this can avoid overfitting concern caused by lack of data and ensured more effective training. Representative features are selected and a large dataset from training the BP ANN model is constructed for expand the applicability and generalization capability of the model.

(2) The BP ANN method successfully predicted the very-high-cycle fatigue life of the Ti-6Al-4V samples with respect to the effect of defect properties and build orientation caused by processing techniques. The BP ANN model effectively seized the failure pattern of the dataset and distinguish one S-N curve caused by characteristic failure features from another and it exempts researchers from laborious traditional experiments.

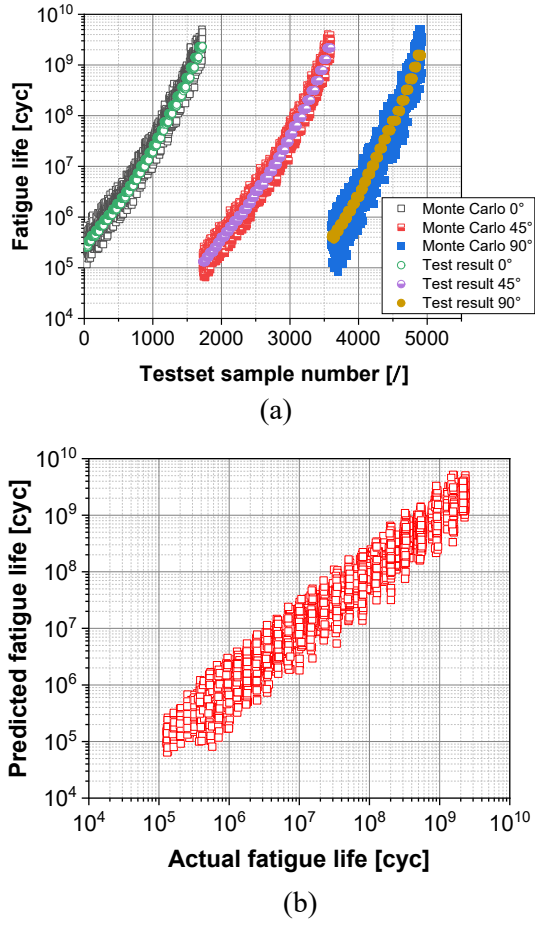

Fig. 9. (a) Fatigue life prediction results compared with MC data; (b) Comparison between the predicted fatigue life by ANN model and the actual fatigue life.

(3) It is found that the BP neural network with L-M learning algorithm exhibits a good fault tolerance and capability in processing very-high-cycle fatigue properties with a high accuracy. The Levenberg-Merquardt learning algorithm has superiority over other learning algorithm for its fast and efficient learning speed in dealing with a large dataset, fast convergence to optimization, and ease of implementation for the code is provided by Matlab.
(4) The accuracy of predicted fatigue curve is limited by the quality of original dataset. Variations or scatter of fatigue properties often cause misinterpretation of interrelationship among variables and thus selection of representative data must be ensured.

Declaration of Competing Interest

The authors declare that they have no known competing financial interests or personal relationships that could have appeared to influence the work reported in this paper.

Acknowledgements

This work was funded by the NSFC Basic Science Center Program for "Multiscale Problems in Nonlinear Mechanics" (No. 11988102), the National Natural Science Foundation of China (No. 11872364, 11932020, 12072345), National Science and Technology Major Project (J2019-VI-0012-0126) and CAS Pioneer Hundred Talents Program.

References

[1] Nicoletto G. Efficient determination of influence factors in fatigue of additive manufactured metals. Procedia Struct Integrity 2018;8:184–91. https://doi.org/10.1016/j.prostr.2017.12.020.
[2] Qian G, Li Y, Paolino DS, Tridello A, Berto F, Hong Y. Very-high-cycle fatigue behavior of Ti-6Al-4V manufactured by selective laser melting: effect of build orientation. Int J Fatigue 2020;136:105628. https://doi.org/10.1016/j.ijfatigue.2020.105628.
[3] Qian G, Jian Z, Qian Y, Pan X, Ma X, Hong Y. Very-high-cycle fatigue behavior of AlSi10Mg manufactured by selective laser melting: effect of build orientation and mean stress. Int J Fatigue 2020;138:105696. https://doi.org/10.1016/j.ijfatigue.2020.105696.
[4] Ben Chaabene W, Flah M, Nehdi ML. Machine learning prediction of mechanical properties of concrete: critical review. Constr Build Mater 2020;260:119889. https://doi.org/10.1016/j.conbuildmat.2020.119889.
[5] Gialanella S, Malandruccolo A. Titanium and titanium alloys. In: Aerospace alloys. Topics in mining, metallurgy and materials engineering. Cham: Springer; 2020. https://doi.org/10.1007/978-3-030-24440-8_4.
[6] Niinomi M. Mechanical properties of biomedical titanium alloys. Mater Sci Eng: A 1998;243(1-2):231–6. https://doi.org/10.1016/S0921-5093(97)00806-X.
[7] Cui C, Hu B, Zhao L, Liu S. Titanium alloy production technology, market prospects and industry development. Mater Des 2011;32(3):1684–91. https://doi.org/10.1016/j.matdes.2010.09.011.
[8] Gardan J. Additive manufacturing technologies: state of the art and trends. Int J Prod Res 2016;54(10):3118–32. https://doi.org/10.1080/00207543.2015.1115909.
[9] Bak D. Rapid prototyping or rapid production? 3D printing processes move industry towards the latter. Assembly Automation 2003;23(4):340–5. https://doi.org/10.1108/01445150310501190.
[10] Hopkinson N, Dickens P. Rapid prototyping for direct manufacture. Rapid Prototyp J 2001;7(4):197–202. https://doi.org/10.1108/EUM0000000005753.
[11] Kasperovich G, Haubrich J, Gussone J, Requena G. Correlation between porosity and processing parameters in TiAl6V4 produced by selective laser melting. Mater Des 2016;105:160–70. https://doi.org/10.1016/j.matdes.2016.05.070.
[12] Liu S, Shin YC. Additive manufacturing of Ti6Al4V alloy: a review. Mater Des 2019;164:107552. https://doi.org/10.1016/j.matdes.2018.107552.
[13] Thijs L, Verhaeghe F, Craeghs T, Humbeeck JV, Kruth J. A study of the microstructural evolution during selective laser melting of Ti–6Al–4V. Acta Mater 2010;V58(9):3303–12. https://doi.org/10.1016/j.actamat.2010.02.004.
[14] Ren S, Chen Y, Liu T, Qu X. Effect of build orientation on mechanical properties and microstructure of Ti-6Al-4V manufactured by selective laser melting. Metall Mater Trans A 2019;V50(9):4388–409. https://doi.org/10.1007/S11661-019-05322-W.
[15] Zhan Z, Li H. A novel approach based on the elastoplastic fatigue damage and machine learning models for life prediction of aerospace alloy parts fabricated by additive manufacturing. Int J Fatigue 2021;145:106089. https://doi.org/10.1016/j.ijfatigue.2020.106089.
[16] Chen H, Yang Y, Cao S, Gao K, Xu S, Li Y, et al. Fatigue life prediction of aluminum alloy 6061 based on defects analysis. Int J Fatigue 2021;147:106189. https://doi.org/10.1016/j.ijfatigue.2021.106189.
[17] Srinivasan V. Low cycle fatigue and creep–fatigue interaction behavior of 316L(N) stainless steel and life prediction by artificial neural network approach. Int J Fatigue 2003;25(12):1327–38.
[18] Nasiri S, Khosravani MR, Weinberg K. Fracture mechanics and mechanical fault detection by artificial intelligence methods: a review. Eng Fail Anal 2017;81:270–93. https://doi.org/10.1016/j.engfailanal.2017.07.011.
[19] Barbosa JF, Correia JAFO, Júnior RCSF, Jesus AMPD. Fatigue life prediction of metallic materials considering mean stress effects by means of an artificial neural network. Int J Fatigue 2020;135:105527. https://doi.org/10.1016/j.ijfatigue.2020.105527.
[20] Bao H, Wu S, Wu Z, Kang G, Peng X, Withers PJ. A machine-learning fatigue life prediction approach of additively manufactured metals. Eng Fract Mech 2021;242:107508. https://doi.org/10.1016/j.engfracmech.2020.107508.
[21] Barbosa JF, Correia JA, Freire Júnior RCS, Zhu S-P, De Jesus AMP. Probabilistic S-N fields based on statistical distributions applied to metallic and composite materials: state of the art. Adv Mech Eng 2019;11(8). https://doi.org/10.1177/1687814019870395.
[22] Xin H, Correia JAFO, Veljkovic M, Zhang Y, Berto F, de Jesus AMP. Probabilistic strain-fatigue life performance based on stochastic analysis of structural and WAAM-stainless steels. Eng Fail Anal 2021;127:105495. https://doi.org/10.1016/j.engfailanal.2021.105495.
[23] Zhu S, Liu Q, Lei Q, Wang Q. Probabilistic fatigue life prediction and reliability assessment of a high pressure turbine disc considering load variations. Int J Damage Mech 2018;V27(10):1569–88. https://doi.org/10.1177/1056789517737132.
[24] Correia JAFO, Huffman PJ, De Jesus AMP, Cicero S, Fernández-Canteli A, Berto F, et al. Unified two-stage fatigue methodology based on a probabilistic damage model applied to structural details. Theor Appl Fract Mech 2017;92:252–65. https://doi.org/10.1016/j.tafmec.2017.09.004.
[25] Shirani M, Härkegård G. Casting defects and fatigue behaviour of ductile cast iron for wind turbine components: a comprehensive study. Materwiss Werksttech 2011;42(12):1059–74. https://doi.org/10.1002/mawe.201100911.
[26] Cevallos-Torres L, Botto-Tobar M. Problem-based learning: a didactic strategy in the teaching of system simulation. Cham: Springer International Publishing; 2019. p. 87–96.

[27] Ribeiro V, Correia J, Mourão A, Lesiuk G, Gonçalves A, De Jesus A, et al. Low-cycle fatigue modelling supported by strain energy density-based Huffman model considering the variability of dislocation density. Eng Fail Anal 2021;128:105608. https://doi.org/10.1016/j.engfailanal.2021.105608.
[28] Zhan Z, Li H. Machine learning based fatigue life prediction with effects of additive manufacturing process parameters for printed SS 316L. Int J Fatigue 2021;142:105941. https://doi.org/10.1016/j.ijfatigue.2020.105941.
[29] Zhang J, Li J, Wu S, Zhang W, Sun J, Qian G. High-cycle and very-high-cycle fatigue lifetime prediction of additively manufactured AlSi10Mg via crystal plasticity finite element method. Int J Fatigue 2022;155:106577. https://doi.org/10.1016/j.ijfatigue.2021.106577.
[30] Qian G, Lei W-S. A statistical model of fatigue failure incorporating effects of specimen size and load amplitude on fatigue life. Phil Mag 2019;99(17):2089–125. https://doi.org/10.1080/14786435.2019.1609707.
[31] Murakami Y, Takagi T, Wada K, Matsunaga H. Essential structure of S-N curve: prediction of fatigue life and fatigue limit of defective materials and nature of scatter. Int J Fatigue 2021;146:106138. https://doi.org/10.1016/j.ijfatigue.2020.106138.
[32] Stein WE, Keblis MF. A new method to simulate the triangular distribution. Math Comput Model 2009;49(5-6):1143–7. https://doi.org/10.1016/j.mcm.2008.06.013.
[33] Davis R. Teaching note—teaching project simulation in excel using PERT-beta distributions. INFORMS Trans Educ 8 (3):139–8. https://doi.org/10.1287/ited.1080.0013.
[34] Sola J, Sevilla J. Importance of input data normalization for the application of neural networks to complex industrial problems. IEEE Trans Nucl Sci 1997;44(3):1464–8. https://doi.org/10.1109/23.589532.
[35] Ramachandra S, Durodola JF, Fellows NA, Gerguri S, Thite A. Experimental validation of an ANN model for random loading fatigue analysis. Int J Fatigue 2019;126:112–21. https://doi.org/10.1016/j.ijfatigue.2019.04.028.
[36] Olawoyin R. Application of backpropagation artificial neural network prediction model for the PAH bioremediation of polluted soil. Chemosphere 2016;161:145–50. https://doi.org/10.1016/j.chemosphere.2016.07.003.
[37] Singh S. Backpropagation learning algorithm based on Levenberg Marquardt algorithm. Comput Sci Inf Technol 2012;2:393–8. https://doi.org/10.5121/csit.2012.2438.
[38] Roweis S. Levenberg-Marquardt Optimization, Computer Science. New York University. https://cs.nyu.edu/~roweis/notes/lm.pdf.
[39] Sharma S, Sharma S, Athaiya A. Activation functions in neural networks. Int J Eng Appl Sci Technol 2020;4(12):310–6. https://doi.org/10.33564/ijeast.2020.v04i12.054.
[40] Apicella A, Donnarumma F, Isgrò F, Prevete R. A survey on modern trainable activation functions. Neural Networks 2021;138:14–32. https://doi.org/10.1016/j.neunet.2021.01.026.
[41] LeCun YA, Bottou L, Orr GB, Müller K. Efficient BackProp. In: Montavon G, Orr GB, Müller KR, editors. Neural networks: tricks of the trade. Lecture notes in computer science, Vol. 7700. Berlin, Heidelberg: Springer; 2012. https://doi.org/10.1007/978-3-642-35289-8_3.